Check for updates

Sensitive dipstick assays for lectin detection, based on glycan–BSA conjugate immobilisation on gold nanoparticles†

Pedro J. Hernando,[a,b] Irina M. Ivanova,[a] Simona Chessa,[a] María J. Marín, [b] Simone Dedola[a,c] and Robert A. Field [b] *[a,c]

There is an unmet need for simple, reliable, and portable devices for the early detection of pathogens and toxins. In this research work, we explored the development of a rapid carbohydrate-based assay for the detection of glycan-binding proteins, lectins, in relation to the detection of the *Ricinus communis* phytotoxin ricin due to its potential as a bioterrorism agent. To allow a visual read-out of the test, gold nanoparticles were applied on a paper-based diagnostic device in the format of a dipstick assay. A small collection of carbohydrates was modified with an azidopropyl tether, allowing the functionalisation of alkyne-modified bovine serum albumin through Cu(I)-catalysed alkyne–azide cycloaddition. To further understand the impact of the nanoparticle size and the presentation of glycans on the assay, *ca.* 150 nm gold nanoshells and *ca.* 40 nm gold nanoparticles covalently functionalised with glycans were investigated for their performance in the dipstick assays. The detection of a selection of lectins, including *R. communis* agglutinin 120, a surrogate for ricin, was carried out. The results presented in this work highlight the potential of glyconanoparticles for the development of cost-effective detection tools for pathogens and toxins bearing surface carbohydrate-binding lectins.

Introduction

The phytotoxin ricin from *Ricinus communis*, present in readily available castor beans,[1] has attracted interest due to its potential as a bioterrorism agent.[2,3] Ricin is fifty times more toxic than cyanide, with a lethal dose in humans estimated at under 20 mg kg^{-1},[4] depending on the exposure route (injection, inhalation through aerosols or ingestion through contaminated food and water).[2,5] Ricin is a heterodimeric protein, consisting of two subunits – the ribosome-inactivating A subunit (RTA) and the galactose/*N*-acetylgalactosamine binding B subunit (RTB), which are linked through a disulfide bond. The widely studied mechanism of action of ricin begins with the binding of the RTB subunit to terminal β-galactoside residues on host cell membranes, allowing the endocytosis of the RTA subunit. This provides RTA with access to ribosomes, which become inactive by selective cleavage of bases from ribosomal RNA, thereby inhibiting protein synthesis.[6]

The detection of ricin, including in samples from crime scenes, is typically achieved by sandwich enzyme-linked immunosorbent assay (ELISA); a combination of gel electrophoresis (SDS-PAGE) and mass spectrometry (MALDI-TOF);[7] or alternatively by lateral flow assays (LFAs), including antibody-based assays with gold nanoparticles (AuNPs)[8,9] or latex particles.[10] Given that RTB is a lectin, efforts have been made to compare the performance of antibodies and glycans for the detection of ricin.[11] For instance, films of either glycosphingolipids or anti-ricin antibodies exposed to RTB showed changes in the infrared spectrum indicating the appearance of amide bonds due to the presence of the lectin. The use of GM1 as a detection probe improved the limit of detection (0.04 μM compared to 0.1 μM with antibodies) and extended the linear range of the assay (0.1–2 μM for the glycan-based assay, compared to 0.5–1 μM for the antibody). Other studies have employed ELISA and surface plasmon resonance (SPR), or SPR imaging of glycan arrays to identify and optimise glycan ligands for use in ricin sensors.[12,13] Such studies often rely on non-toxic *R. communis* agglutinin 120 (RCA$_{120}$) as a practical surrogate for ricin.[14–16] For convenience, albeit still lab-based, glyconanoparticles have been deployed in colorimetric aggregation-based bioassays for the detection of ricin[17,18] and

[a]*Iceni Glycoscience, Norwich Research Park, Norwich NR4 7GJ, UK*
[b]*School of Chemistry, University of East Anglia, Norwich Research Park, Norwich NR4 7TJ, UK*
[c]*School of Chemistry and Manchester Institute of Biotechnology, University of Manchester, Manchester M1 7DN, UK. E-mail: robert.field@manchester.ac.uk*
†Electronic supplementary information (ESI) available. See DOI: https://doi.org/10.1039/d3qo00424d

This journal is © the Partner Organisations 2023

Org. Chem. Front., 2023, **10**, 3819–3829 | 3819

cholera toxin,[19] and for the detection and discrimination between human and avian influenza viruses,[20] for instance.

Glyconanoparticle-based flow assays have been developed for the detection of pathogens, such as SARS-CoV-2.[21–23] These assays are based on nitrocellulose strips with a deposited capturing agent (test line) and a AuNP-based detection agent. A sample containing the target analyte runs along the strip and, in the presence of a specific analyte, a visual test line appears upon formation of a sandwich-like interaction between the capturing agent, the given lectin or pathogen analyte, and the AuNPs. Glyconanoparticle-based dipstick assays have also been optimised in terms of galactose presentation[24] for the detection of RCA$_{120}$ and soybean agglutinin, providing limits of detection around 0.5 mg mL^{-1}.

The optical properties of metal nanoparticles, which arise from the oscillation of surface electrons interacting with an electromagnetic field,[25] are affected by the metal core, its size and shape.[26–28] Experimental and theoretical studies have shown that nanoparticles of increasing sizes can improve the sensitivity of LFAs.[29,30] However, although a higher diameter/surface area enables a higher degree of functionalisation, this also brings technical issues related to the diffusion of the particles throughout the nitrocellulose strip. Examples of the use of core–shell silica–gold nanoshells (AuNSs) for LFAs have been reported, where antibodies were used for the functionalisation of ca. 100 nm AuNSs for the detection of nematode immunogenic peptides[31] or myxovirus resistance protein A.[32]

The application of carbohydrates in a rapid detection platform based on the principle of LFAs was recently reviewed by Gibson et al.,[16] and includes reports on the translation of glyconanoparticle aggregation assays into a nitrocellulose-based chromatographic assay format. Toyoshima et al.[33,34] reported the detection of Shiga toxin 1 and Concanavalin A (ConA) with mannose-functionalised nanoparticles, while Baker et al.[21,22] reported the detection of SARS-CoV-2 virus from clinical samples using N-acetyl neuraminic acid-functionalised poly (hydroxyethyl acrylamide) AuNPs, and Kim et al.[35] used glycosaminoglycans as the capturing agent on a test line for a SARS-CoV-2 LFA.

AuNPs can be functionalised with synthetic approaches that result in the covalent or non-covalent functionalisation of the gold surface with the glycans. All such functionalisation strategies reported to date present advantages and disadvantages,[36] and the choice will depend on the final application and use of the glyconanoparticles. Thiol-derivatised carbohydrates[19,37–39] and thioctic acid derivatives[40] have been extensively reported for AuNPs functionalised with well-defined glycans. A different approach on the assembly of glyconanoparticles is the use of AuNPs functionalised with a non-glyco-ligand to which the desired carbohydrate is reacted to form a covalent bond via, for example, simple carbodiimide chemistry,[41] or reductive amination.[42] Non-covalent approaches to the functionalisation of AuNPs include the use of glycopeptides,[43] direct incorporation of polysaccharides through their hydroxyl groups via oxygen-to-gold dative bond,[44] or functionalisation with proteins as reported in this paper. One of the disadvantages of non-covalent functionalisation is that the interactions between the gold surface and the ligand rely on electrostatic interactions, which can be influenced by pH or ionic strength. Therefore, any assay condition that may impact on such electrostatic interactions could interfere with the functionalisation and stability of the nanoparticles. The non-covalent functionalisation also offers less control of the ligand orientation and, consequently presentation to the target protein/lectin or pathogen is harder to predict.[45]

In the present study, we report a comparison between 40 nm AuNPs and 150 nm AuNSs for the detection of RCA$_{120}$ in a simple dipstick assay format, in lieu of a full LFA. We also present a comparison of three types of nanomaterials: bovine serum albumin (BSA)-functionalised 40 nm AuNPs; 40 nm AuNPs and 150 nm AuNSs decorated with galactose residues.

The comparison and binding assessment of the carbohydrate panel provided an evaluation of the selectivity against the chosen lectins and could be used to rationalise and rule out cross-reactions, hence interference, in the final assay of RCA$_{120}$ detection. The evaluation also provided a basis for further development of LFA-based assays for toxins or pathogens detection.

Results

For initial studies, we selected a range of carbohydrates that could serve as appropriate controls, with known and well characterised carbohydrate–lectin interaction. Besides galactose and lactose, to be employed for the detection of RCA$_{120}$, we selected mannose and α3,α6-mannotriose, to be tested against ConA but also relevant to bacterial adhesion, and 3′-sialyllactose to be tested against WGA and potentially relevant to respiratory viruses. A glucose derivative was included in the panel as a negative control against all the employed lectins. To standardise the evaluation process, we selected a simple and short azidopropyl linker for all the carbohydrate moieties, for use with copper-catalysed azide–alkyne cycloaddition (CuAAC) "click chemistry" functionalisation.[46,47]

The carbohydrate probes in this study were first conjugated to BSA, which serves as a versatile support allowing multivalent presentation of the sugars and, exploiting its hydrophobicity, for immobilisation of the glycoconjugates onto nitrocellulose or nanoparticles by passive adsorption.[48] The CuAAC conjugation methodology[49,50] enabled coupling of the azide installed on the sugar and an alkyne counterpart on the BSA. The installation of the alkyne functional group on the BSA was achieved by using the glycidyl propargyl ether, a readily available and low-cost reagent that has little used to date in this context. Although bioconjugation methods targeting lysine had been extensively investigated in recent years,[51,52] epoxy-based derivatisation agents are not widely used, with only sporadic recent examples. In the context of carbohydrates, the glycidyl propargyl ether has been used to generate functionalised mannose polymers after the polymerisation of the

3820 | Org. Chem. Front., 2023, 10, 3819–3829

This journal is © the Partner Organisations 2023

epoxide, which generated a multi-alkyne functional polyethylene glycol, followed by CuAAC with mannose azide.[53] Epoxides can react with primary amines, sulfhydryl or hydroxyl groups to create secondary amines, thioethers or ether bonds, respectively. The epoxide opening reaction in the presence of a primary amine results in the formation of a secondary amine, for example when reacted with a lysine side chain, providing a lower impact on the surface charge of a protein if compared with the more popular amide-forming NHS-activated reagents. Considering that cysteine residues in BSA are engaged in disulphide and are buried internally, epoxide reagents are likely to target mainly the more reactive primary amine on the protein surface. For the installation of glycans on the surface of BSA, available lysine residues have been targeted in the past through direct glycation[54,55] leading to BSA with glycans directly attached through their reducing ends. Recently, BSA has been functionalised with galactose employing very short spacers such as thiophosgene[56] or squaramide,[57] as well as a longer PEG.[58] These approaches often aim at forming a neutral amide linkage between the ligand and BSA, whereas epoxide-opening chemistry leads to the formation of a protonatable secondary amine and a primary alcohol, which is less disruptive in terms of hydrogen bond-forming and solubility of the resulting glycoconjugate.

Synthesis of glycosides and bovine serum albumin glycoconjugates

Azidopropyl glycoside derivatives of galactose (Gal, **1**), lactose (Lac, **2**), glucose (Glc, **3**), mannose (Man, **4**) and 3,6-di-*O*-α-mannopyranosyl-α-mannopyranose (α3α6-Man, **5**) were prepared following published synthetic routes and the final structures are shown in Fig. 1A. Briefly, peracetylated galactose, lactose and glucose[50] were coupled to 3-azidopropan-1-ol *via*

$BF_3 \cdot OEt_2$-promoted glycosylation[59] to afford acetylated azidopropyl galactoside (**1**), lactoside (**2**), and glucoside (**3**), respectively, which were deprotected *via* Zemplen deacetylation.

The mannoside derivative was obtained following a different methodology, to afford higher chemical yields. Briefly, the synthesis was performed starting from perbenzoylated mannose[63] and subsequent bromination at the anomeric position[64] to obtain the corresponding benzoylated mannosyl bromide donor that was directly used for glycosylation with 3-azidopropan-1-ol promoted by AgOTf.[61] This gave the desired glycoside (**4**) after deprotection under Zemplen conditions. Selective partial benzoylation of (**4**) was achieved through *ortho*-ester chemistry,[61] to afford azidopropyl 2,4-di-*O*-benzoyl mannoside. ^{1}H-NMR allowed the unambiguous identification of the desired product, based on the diagnostic chemical shift of the protected 4-position at 5.5 ppm, in comparison with an analogous compound reported by Oscarson *et al.*,[61] with a chemical shift of the 4-position at 5.8 ppm. That work also reported the data for the 2,6-di-*O*-benzoyl mannoside, with a chemical shift of the 4-position at 3.9 ppm, which allowed to distinguish between both isomers. The partially protected mannoside was successively submitted to AgOTf-promoted glycosylation with benzoylated mannosyl bromide to afford benzoylated azidopropyl mannose-α-1,3-(mannose-α-1,6-)mannoside (**5a**, in ESI†), which was then deprotected to afford the 1,3/6-linked azidopropyl mannotrioside (α3α6-Man, **5**). Specific installation of sialic acid at the 3′ position of lactoside **2** was performed using *Trypanosoma cruzi trans*-sialidase and fetuin as the sialic acid donor,[65] affording azidopropyl 3′-sialyllactoside (3′SL, **6**).

As judged by MALDI-TOF mass spectrometry, the propargyl-functionalised BSA (**7**) was synthesised with nearly full conversion of its 30–35 available lysine residues (out of 59 lysines)[66]
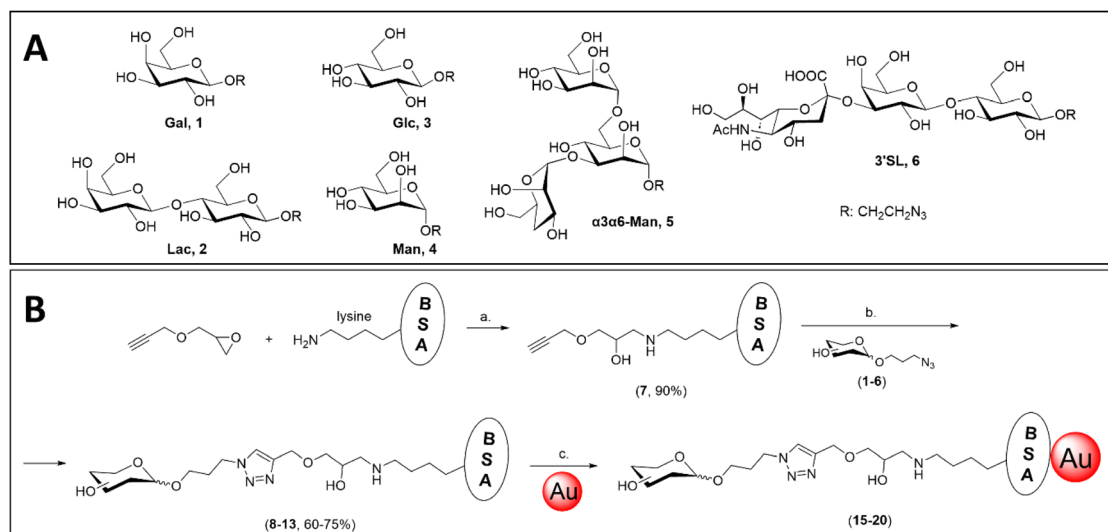

Fig. 1 (A) Azidopropyl glycosides synthesised in this work, including a β-galactoside (Gal, **1**),[60] β-lactoside (Lac, **2**),[60] β-glucoside (Glc, **3**),[59] α-mannoside (Man, **4**),[61] 3,6-di-*O*-α-mannopyranosyl-α-mannopyranoside (α3α6-Man, **5**)[61] and α-2,3′-sialyllactoside (3′SL, **6**).[62] (B) Synthesis of BSA glycoconjugates following epoxide-opening chemistry, and subsequent passive adsorption on the surface of gold nanoparticles. Reagents and conditions: (a) $NaHCO_3$ (aq., 10 mM), 37 °C, o.n.; (b) Cu_2SO_4, THPTA, NaAsc, 37 °C, o.n.; (c) citrate buffer (2 mM, pH 5.3), r.t., o.n.

This journal is © the Partner Organisations 2023

Org. Chem. Front., 2023, **10**, 3819–3829 | **3821**

Table 1 MALDI-TOF-MS data for all the BSA conjugates synthesised in this work. MW: molecular weight (Da)

Ligand	MW ligand	ΔMW	Average ligands per BSA	Ligand	MW ligand	ΔMW	Average ligands per BSA
Propargyl ether (7)	112	3197	29	Man (4)	263	2181	8
Gal (1)	263	825	3	α3α6-Man (5)	587	1626	3
Lac (2)	425	3214	8	3′SL (6)	716	2354	3
Glc (3)	263	1626	6				

to propargyl moieties, following epoxide-opening chemistry with propargyl glycidyl ether (Fig. 1B). Subsequent CuAAC afforded the library of BSA glycoconjugates including Gal-BSA (**8**), Lac-BSA (**9**), Glc-BSA (**10**), Man-BSA (**11**), α3α6-Man-BSA (**12**) and 3′SL-BSA (**13**). All the BSA glycoconjugates were analysed by MALDI-TOF-MS, where the average number of glycans per BSA unit was evaluated by the difference in molecular weight between product and starting material, as reported in Table 1. Full MALDI-TOF-MS spectra are reported in the ESI, Fig. S1–S8.†

Functionalisation of citrate-capped 40 nm AuNPs with BSA glycoconjugates

Standard passive adsorption of the BSA conjugates onto 40 nm AuNPs was performed (Fig. 1B) to afford propargyl-BSA-AuNPs (**14**), Gal-BSA-AuNPs (**15**), Lac-BSA-AuNPs (**16**), Glc-BSA-AuNPs (**17**), Man-BSA-AuNPs (**18**), α3α6Man-BSA-AuNPs (**19**) and 3′SL-BSA-AuNPs (**20**). The derivatised nanoparticles were characterised by transmission electron microscopy (TEM), dynamic light scattering (DLS) and UV-Vis absorption spectroscopy (refer to Table S3 and Fig. S9† for full characterisation data). Some variability was found in the size measured by TEM in the AuNPs **14** (39 ± 0.5 nm) and **15** (42 ± 0.4 nm); however, this was in agreement with the specifications given by the provider of the citrate-capped AuNPs (40 ± 4 nm). Analysis of the UV-Vis spectra of the set of glyconanoparticles showed a shift of the maximum of absorbance between 2 and 3 nm from the non-functionalised AuNPs, which is an indication of the successful functionalisation,[67] as the absorbance is directly impacted by the surface coating of the AuNPs. DLS data for the set of nanoparticles showed an increase in hydrodynamic diameter between 7 and 8 nm following functionalisation, again indicating the successful modification of the nanoparticle surfaces with BSA conjugates.

Performance of glycan–BSA-functionalised 40 nm AuNPs in dipstick assays

The specific interactions between the library of glyconanoparticles (**15**)–(**20**) and a selection of lectins were investigated using a dipstick assay format, schematically reported in Fig. 2 (see also Fig. S11†). Briefly, the lectin of interest was deposited onto a nitrocellulose strip, which was then conditioned by eluting 20 μL of a running solution composed of 10 mM phosphate buffer (PB), 1% polyvinylpyrrolidone (PVP), 50 mM NaCl and 0.05% Tween-20. To assess the binding, a solution of the functionalised AuNPs was allowed to flow along the strip to develop a visual signal where the lectin was deposited.
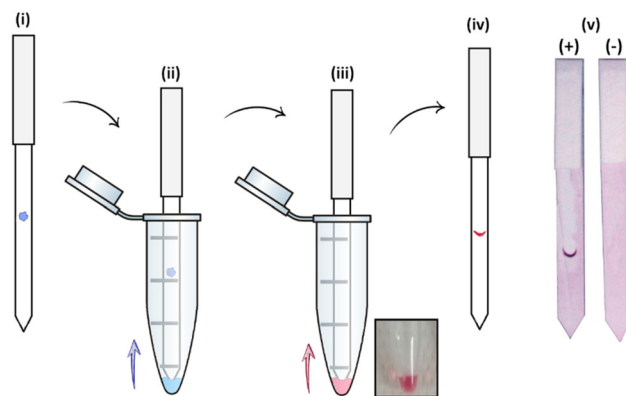

Fig. 2 Workflow scheme of the dipstick assay: (i) the lectin is deposited on the nitrocellulose strip, (ii) which is conditioned with 20 μL of running buffer. (iii) The functionalised AuNPs are flown through the strip, to (iv) develop a visual signal upon interaction with the lectin. (v) Representative images of a (+) positive and a (−) negative dipstick assay result.

The range of lectins assessed included RCA$_{120}$ (galactose-binding), wheat germ agglutinin (WGA, sialic acid-binding) and ConA (mannose-binding; weak glucose-binding). Controls were performed with propargyl-BSA-AuNPs (**14**) to exclude non-specific interactions. Each dipstick was imaged using a gel imager and the signals were normalised against the dipstick signal intensity for the detection of RCA$_{120}$ (2.5 μg) with Gal-BSA-AuNPs (**15**) (OD 1). All the experiments were performed in triplicate for statistical treatment of the results. Representative data for the dipstick assays are presented in Fig. 3, underneath the corresponding data.

Covalent functionalisation of 40 nm AuNPs and 150 nm AuNSs with galactose

To study the effect of BSA and compare the difference between passive adsorption and covalent functionalisation, commercially available ca. 40 nm NHS ester-activated AuNPs were coupled with 3-aminopropyl galactoside **21**, obtained by reduction of **1**,[68] to afford Gal-AuNPs (**22**, Fig. 4).

The optimisation of the covalent functionalisation of AuNSs was performed as a systematic investigation of pH, time, and ligand concentration (selected data shown in Fig. 5; refer to the ESI† for the full data). The functionalised AuNSs were assessed using the same dipstick assay format employed for the corresponding nanoparticles shown in Fig. 2. Upon functionalisation at pH 6, the AuNSs did not show any interaction with the RCA$_{120}$ even after 24 h of functionalisation. At
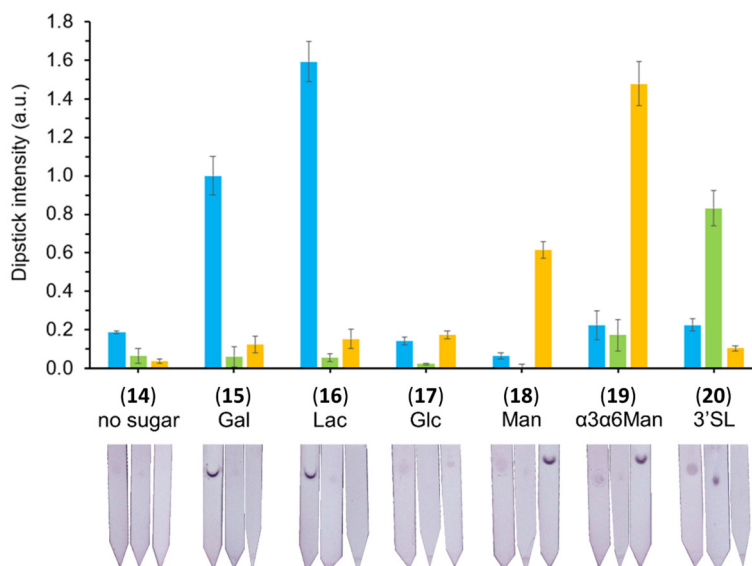
Fig. 3 Selectivity studies on the detection of lectins, glyconanoparticles (OD 1) functionalised *via* passive adsorption with either of the different glycan–BSA conjugates (**15–20**). The glyconanoparticles were screened for the detection of 2.5 µg of either RCA_{120} (blue), WGA (green) and ConA (yellow). Controls were performed with propargyl-BSA-AuNPs (**14**) against the respective lectins. Error bars indicate the standard deviation of the triplicates in the experiment. The signal intensities were quantified, divided by the loading of glycans per BSA presented in Table 1, and normalised against the detection of 2.5 µg of RCA_{120} with Gal-BSA-AuNPs (**15**). Below each set of data, the image of a representative dipstick is presented.
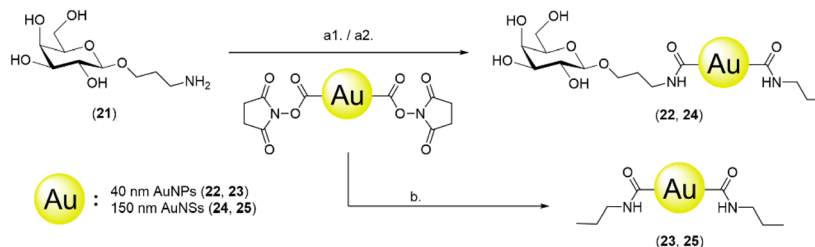

Fig. 4 Pathway for the covalent functionalisation of NHS-activated particles with aminopropyl galactoside **21**. Reagents and conditions: (a1) HEPES buffer 10 mM pH 8.0, 0.5% PEG-20k, 6 h, r.t.; (a2) propylamine, 10 min; and (b) propylamine, HEPES buffer 10 mM pH 8.0, 0.5% PEG-20k, 6 h.

pH 7.4 the development of a weak signal confirmed binding of the AuNSs to the deposited lectin with an increase in intensity with the time of functionalisation. At pH 8.0, weak binding
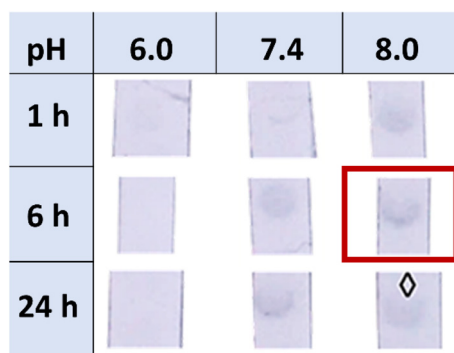

Fig. 5 Dipstick matrix images for the optimisation of the AuNSs functionalisation using different functionalisation times (1 h, 6 h, or 24 h) and pHs (6, 7.4, or 8).

was observed already after 1 h of functionalisation, with an optimal signal observed after functionalisation for 6 h. After 24 h, the particles performance decreased showing aggregation and precipitation at the bottom of the nitrocellulose strip. Overall, the results obtained at pH 8.0 and 6 h were comparable to the one obtained at pH 7.4 and 24 h. Given the shorter reaction time, pH 8.0 and 6 h were selected as optimal conditions for the AuNSs functionalisation.

The conditions for the functionalisation were optimised to pH 8.0 and 6 h, employing 0.1 mM glycoside (see the ESI† for the description of the optimisation process). NHS ester-activated AuNPs were also directly quenched with propylamine to obtain propyl-AuNPs (**23**), to be used as negative control in the dipstick assay. Gal-AuNPs (**22**) were characterised by TEM, DLS and UV-vis (Fig. S10†) and the data were compared to those for commercial 40 nm NHS ester-activated AuNPs.

To explore the impact of the nanoparticle size in the assay, a 150 nm glyconanoshell system was also evaluated. The AuNSs were functionalised with 3-aminopropyl galactoside

This journal is © the Partner Organisations 2023

Org. Chem. Front., 2023, **10**, 3819–3829 | **3823**

(**21**), as described above for nanoparticle derivatisation, to afford galactose-functionalised AuNSs (**24**) (Fig. 4). The conditions for the functionalisation were optimised to pH 8.0 and 6 h, employing 1 mM glycoside (see the ESI† for the description of the optimisation process). NHS ester-activated AuNSs were also directly quenched with propylamine to obtain propyl-AuNSs (**25**), to be used as negative control in the dipstick assay. The Gal-AuNSs (**24**) were characterised by TEM, DLS and UV-Vis (Fig. S10†) and the data were compared to those for commercial 150 nm NHS ester-activated AuNSs.

Sensitivity studies and comparison of particle performance

The sensitivity of the three glyconanosystems was investigated in a dipstick assay format, with a dilution series of RCA_{120} starting from 2500 ng down to 2.5 ng. To assess the performance of the different detection agents in the dipstick assay, only the 150–0 ng range was quantified (Fig. 6). Images of the full range of dipsticks can be found in the ESI (Fig. S17†). We found that the AuNPs and AuNSs covalently functionalised with galactose (**23** and **24**) had a visual limit of detection of *ca.* 75 ng of RCA_{120}, whereas the BSA-Gal-AuNPs could detect down to 20 ng. Despite most of the available lysine have been functionalised with an alkyne moiety (average of 29), the number of glycans that we were able to install on the BSA was

relatively low. Prompted by the performance of Gal_3-BSA-AuNPs (**15**), we decided to focus our effort in trying to increase the glycan loading on the Gal-BSA glycoconjugate, which was the key conjugate of interest for the detection of RCA_{120}. It has been reported that protecting the reaction mixture from oxygen can improve the performance of the CuAAC.[69] While the catalytic amount of Cu(ɪ) formed *in situ* by the reductive action of sodium ascorbate is generally sufficient to drive the "click" reaction to completion in short time, in our hands the reaction was left over night, requiring an extended availability of Cu(ɪ). Degassed water was used to prepare all the reagent solutions and for the reaction mixture. Using this approach, we obtained a new BSA-glycoconjugate with a higher density of galactose (Gal_{14}-BSA, **8a**), which was characterised through MALDI-TOF showing 14 galactose units instead of 3 (Fig. S8†). This glycoconjugate was employed for the functionalisation of AuNPs through passive adsorption to obtain Gal_{14}-BSA-AuNPs (**15a**), which were applied in the dipstick assay. It was found that an approximate 4-fold increase in glycan density on the BSA glycoconjugate improved the sensitivity of the assay by a similar factor, being able to detect down to 5 ng of RCA_{120} (Fig. 6). The comparison shows visually that the glycan-BSA-AuNP construct out-performs other options investigated in terms of sensitivity.

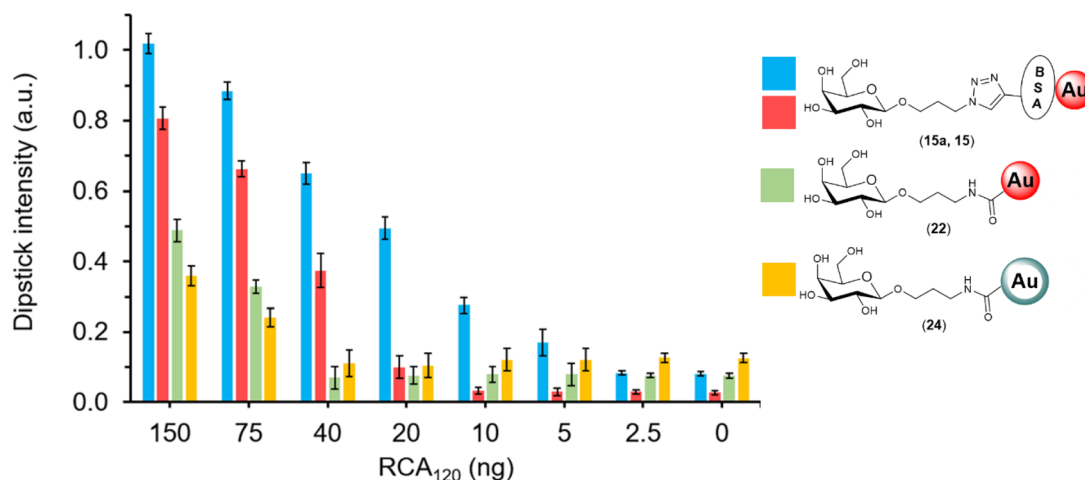**Fig. 6** Sensitivity studies using 40 nm AuNPs (OD 1) functionalised *via* passive adsorption with either Gal_{14}-BSA (**15a**, blue) or Gal_3-BSA (**15**, red), 40 nm AuNPs covalently functionalised with galactose (**22**, green) or 150 nm AuNSs covalently functionalised with galactose (**24**, yellow) to detect different amounts of RCA_{120}. The dipsticks were analysed in the 150–2.5 ng range and signal intensities were quantified and normalised against a dipstick signal for the detection of 2500 ng of RCA_{120} with **15**. Error bars show the standard deviation between triplicates.

Table 2 Comparison of limits of detection for RCA_{120}, RTA, RTB or ricin in flow systems

Analyte	Type of ligand	Reported LOD	Absolute amount detected (ng¦fmol)	Tested range	Ref.
RCA_{120}	Glycan	5 ng	5¦39	2.5–2500 ng	This work
RTA	Antibody	33 ng mL^{-1}	2.3¦72	5–1000 ng mL^{-1}	10
RCA_{120}	Antibody	135 ng mL^{-1}	9.5¦73	5–1000 ng mL^{-1}	10
Ricin	Antibody	35 µg mL^{-1}	9.6¦148	0.01–10 µg mL^{-1}	9
RTB	Antibody	870 ng mL^{-1}	60.9¦1791	5–1000 ng mL^{-1}	10
RCA_{120}	Glycan	0.5 mg mL^{-1}	500¦3846	5–0.1 mg mL^{-1}	24

3824 | *Org. Chem. Front.*, 2023, **10**, 3819–3829

This journal is © the Partner Organisations 2023

Discussion and conclusions

AuNPs with diameters of *ca.* 40 nm are typically the favoured colorimetric labels for LFAs. This is due to the convenient combination of high contrast red colour, available surface area for functionalisation (as opposed to smaller nanoparticles), and long stability (as opposed to bigger nanoparticles). In the present work, we opted for passive adsorption of BSA glycoconjugates (**8–13**) on the surface of commercially available *ca.* 40 nm AuNPs, to obtain a collection of BSA-glyconanoparticles (**15–20**). The results from DLS presented in Fig. S9 and Table S3† showed an average increase of the particle size of 7–8 nm following functionalisation, which reflects an approximate single layer of BSA conjugates (BSA dimensions[70] 7.5 × 6.5 × 4 nm) on the surface of the nanoparticles.

The binding specificities of the lectins selected for this work are well known in the literature: RCA_{120} interacts with terminal β-galactosides,[71] WGA interacts with sialic acids,[72] and ConA interacts with α-mannosides (more specifically with α3,α6-mannotrioside).[73] To account for the difference in glycan loading of each glycoconjugate, the signal intensity of each dipstick was divided by the number of glycan units of each BSA glycoconjugate construct used in experiments presented in Fig. 3. Each of the BSA-bearing glyconanoparticles (**15**)–(**20**) successfully detected the lectin of matching selectivity.

To further investigate the optimal distribution of glycans for the detection system, 3-aminopropyl galactoside (**21**) was synthesised following Staudinger reduction of azidopropyl galactoside **1** and was subsequently coupled to NHS-ester activated AuNPs, to obtain Gal-AuNPs (**22**). Due to the similarity with the aminopropyl ligands employed, propylamine was chosen as an appropriate reagent to quench unreacted NHS-ester. Propyl-functionalised AuNPs (**23**) were also prepared and tested as a negative control to verify the absence of non-specific interactions (dipsticks images in Fig. S15A†). In addition, 150 nm NHS ester-activated AuNSs were chosen to investigate the effect that the size has on the detection system, as these exhibit a 14 times bigger surface area than 40 nm AuNPs, which can lead to up to 25 times improved sensitivity in immunochromatographic assays.[74,75] Propyl-AuNSs (**25**) were prepared as negative controls by quenching AuNSs in absence of the galactoside, to study non-specific interactions with RCA_{120} and WGA. Non-specific interactions were observed between the nanoshells and both RCA_{120} and WGA, which was overcome by the addition of a combination of 1% Triton X100 and 1% BSA to the dipstick buffer.

Following the optimisation of the three different nanosystems, a series of experiments were performed to evaluate their relative sensitivity for RCA_{120} detection. For this purpose, dipsticks were generated with defined amounts of RCA_{120} ranging from 2.5–150 ng. These assays demonstrated that BSA-mediated presentation of glycans on the surface of AuNPs allows an optimal presentation of glycans, even though the sugar loading is expected to be much lower than for direct covalent attachment of sugars to gold nanoparticles or nano-

shells. It has been noted before that glycan density on the surface of nanoparticles is a key parameter to tune when designing a glyconanoparticle-based sensing system and that more sugar does not necessarily equate with greater assay sensitivity.[76]

Prompted by the performance of the BSA-glyconanoparticles, a new Gal-BSA glycoconjugate was synthesised, Gal_{14}-BSA (**8a**), containing 14 glycan units instead of 3, as for Gal_3-BSA (**8**). The glyconanoparticles functionalised with the new glycoconjugate (Gal_{14}-BSA-AuNPs, **15a**) were applied to the dipstick assay, giving rise to a lower limit of detection (5 ng of RCA_{120}).

In summary, the BSA-based glycan presentation method presented here resulted in reproducible functionalisation of nanomaterials which were implemented in a dipstick assay for the detection of plant lectins. A potential detection system for ricin has been developed in the format of a dipstick assay, using RCA_{120} as a model of binding due to its lack of toxicity. Three different glyconanomaterials have been successfully synthesised, including 40 nm AuNPs (functionalised through BSA *via* passive adsorption), 40 nm AuNPs (covalently functionalised *via* NHS ester coupling) and 150 nm AuNSs (covalently functionalised *via* NHS ester coupling). All the functionalised nanoparticles have been tested against different lectins to demonstrate their specificity in a dipstick format. From these studies we conclude that BSA-bearing 40 nm AuNPs are optimal agents for the detection of lectins, with a working range of 150–2.5 ng and a LOD of 5 ng for RCA_{120}, which is lower than that reported to date for other flow-based RCA_{120}/RTA/RTB/ricin assays, including those reliant on antibody for target engagement (Table 2).

This proof-of-concept study showed the potential of glyconanoparticles as an alternative approach to classic reagents employed in standard immunochromatographic assays. The BSA-glycoconjugates can be used as detection reagents on nanoparticles or as capture reagents deposited onto the nitrocellulose strip for a conventional sandwich assay. In the present work, the direct detection of the analyte deposited on the nitrocellulose strip provided the proof of concept to validate the achievable limit of detection and operating range as a combination of functionalisation methodology, nanoparticle type and size. Although the direct deposition of a clinical or environmental sample on the dipstick/LFA is possible, it would require high precision liquid dispensing device in order to achieve accurate and reliable outcomes, which would be challenging in the field. The optimisation of the newly reported epoxy-based approach for protein functionalisation and the translation of the assay in a full sandwich dipstick/LFA assay format will, with or without partner antibody reagents, form the basis of future work.

Methods

The ESI† contains details about the synthesis of glycan derivatives, derivatisation of bovine serum albumin and functionalisation of gold nanoparticles and nanoshells.

This journal is © the Partner Organisations 2023

Org. Chem. Front., 2023, **10**, 3819–3829 | **3825**

Author contributions

PJH performed the experimental work described in this paper, analysed the data, wrote the original manuscript draft and contributed to reviewing and editing. IMI contributed to the design of experiments and analysis of the data regarding gold nanoparticles, nanoshells and dipsticks. SC contributed to the optimisation of the functionalisation of bovine serum albumin, passive adsorption on gold nanoparticles and to the expression and purification of *T. cruzi trans*-sialidase. SD and MJM contributed to the supervision of the project as well as the revision and editing of the manuscript. RAF designed this project, supervised this research project, and contributed to the revision of the manuscript.

Conflicts of interest

Iceni Glycoscience Ltd is developing glyconanoparticle approaches for diagnostic use.

Acknowledgements

References

1 S. Worbs, K. Köhler, D. Pauly, M. A. Avondet, M. Schaer, M. B. Dorner and B. G. Dorner, Ricinus communis intoxications in human and veterinary medicine-a summary of real cases, *Toxins*, 2011, **3**, 1332–1372.

2 G. A. Balint, Ricin: the toxic protein of castor oil seeds, *Toxicology*, 1974, **2**, 77–102.

3 E. Janik, M. Ceremuga, J. S. Bijak and M. Bijak, Biological toxins as the potential tools for bioterrorism, *Int. J. Mol. Sci.*, 2019, **20**, 1181.

4 F. Musshoff and B. Madea, Ricin poisoning and forensic toxicology, *Drug Test. Anal.*, 2009, **1**, 184–191.

5 J. Audi, M. Belson, M. Patel, J. Schier and J. Osterloh, Ricin Poisoning A Comprehensive Review, *J. Am. Med. Assoc.*, 2005, **294**, 2342–2351.

6 J. M. Lord, L. M. Roberts and J. D. Robertus, Ricin: structure, mode of action, and some current applications, *FASEB J.*, 1994, **8**, 201–208.

7 S. Simon, S. Worbs, M. A. Avondet, D. M. Tracz, J. Dano, L. Schmidt, H. Volland, B. G. Dorner and C. R. Corbett, Recommended immunological assays to screen for ricin-containing samples, *Toxins*, 2015, **7**, 4967–4986.

8 R.-H. Shyu, H.-F. Shyu, H.-W. Liu and S.-S. Tang, Colloidal gold-based immunochromatographic assay for detection of ricin, *Toxicon*, 2002, **40**, 255–258.

9 J. Dayan-Kenigsberg, A. Bertocchi and E. A. E. Garber, Rapid detection of ricin in cosmetics and elimination of artifacts associated with wheat lectin, *J. Immunol. Methods*, 2008, **336**, 251–254.

10 R. E. Fulton and H. G. Thompson, Fluorogenic hand-held immunoassay for the identification of ricin: Rapid analyte measurement platform, *J. Immunoassay Immunochem.*, 2007, **28**, 227–241.

11 R. Stine, M. v. Pishko and C. L. Schengrund, Comparison of glycosphingolipids and antibodies as receptor molecules for ricin detection, *Anal. Chem.*, 2005, **77**, 2882–2888.

12 S. S. Mahajan and S. S. Iyer, ELISA and SPR Studies of Ricin Binding to β-Galactoside Analogs, *J. Carbohydr. Chem.*, 2012, **31**, 447–465.

13 M. Fais, R. Karamanska, S. Allman, S. A. Fairhurst, P. Innocenti, A. J. Fairbanks, T. J. Donohoe, B. G. Davis, D. A. Russell and R. A. Field, Surface plasmon resonance imaging of glycoarrays identifies novel and unnatural carbohydrate-based ligands for potential ricin sensor development, *Chem. Sci.*, 2011, **2**, 1952–1959.

14 S. Sharma, S. Bharadwaj, A. Surolia and S. K. Podder, Evaluation of the stoichiometry and energetics of carbohydrate binding to *Ricinus communis agglutinin*: a calorimetric study, *Biochem. J.*, 1998, **333**, 539–542.

15 R. Macholz, The Lectins., Properties, Functions, and Applications in Biology and Medicine, *Mol. Nutr. Food Res.*, 1988, **32**, 212–213.

16 A. N. Baker, G. W. Hawker-Bond, P. G. Georgiou, S. Dedola, R. A. Field and M. I. Gibson, Glycosylated gold nanoparticles in point of care diagnostics: from aggregation to lateral flow Antibody-based lateral flow, *Chem. Soc. Rev.*, 2022, **51**, 7238–7259.

17 C. L. Schofield, B. Mukhopadhyay, S. M. Hardy, M. B. McDonnell, R. A. Field and D. A. Russell, Colorimetric detection of Ricinus communis Agglutinin 120 using optimally presented carbohydrate-stabilised gold nanoparticles, *Analyst*, 2008, **133**, 626–634.

18 M. J. Marín, C. L. Schofield, R. A. Field and D. A. Russell, Glyconanoparticles for colorimetric bioassays, *Analyst*, 2015, **140**, 59–70.

19 C. L. Schofield, R. A. Field and D. A. Russell, Glyconanoparticles for the colorimetric detection of cholera toxin, *Anal. Chem.*, 2007, **79**, 1356–1361.

20 M. J. Marín, A. Rashid, M. Rejzek, S. A. Fairhurst, S. A. Wharton, S. R. Martin, J. W. McCauley, T. Wileman, R. A. Field and D. A. Russell, Glyconanoparticles for the plasmonic detection and discrimination between human and avian influenza virus, *Org. Biomol. Chem.*, 2013, **11**, 7101–7107.

21 A. N. Baker, S. J. Richards, S. Pandey, C. S. Guy, A. Ahmad, M. Hasan, C. I. Biggs, P. G. Georgiou, A. J. Zwetsloot, A. Straube, S. Dedola, R. A. Field, N. R. Anderson, M. Walker, D. Grammatopoulos and M. I. Gibson, Glycan-Based Flow-Through Device for the Detection of SARS-COV-2, *ACS Sens.*, 2021, **6**, 3696–3705.

3826 | *Org. Chem. Front.*, 2023, **10**, 3819–3829

This journal is © the Partner Organisations 2023

22 A. N. Baker, S. J. Richards, C. S. Guy, T. R. Congdon, M. Hasan, A. J. Zwetsloot, A. Gallo, J. R. Lewandowski, P. J. Stansfeld, A. Straube, M. Walker, S. Chessa, G. Pergolizzi, S. Dedola, R. A. Field and M. I. Gibson, The SARS-COV-2 Spike Protein Binds Sialic Acids and Enables Rapid Detection in a Lateral Flow Point of Care Diagnostic Device, *ACS Cent. Sci.*, 2020, **6**, 2046–2052.

23 A. N. Baker, T. R. Congdon, S.-J. Richards, P. G. Georgiou, M. Walker, S. Dedola, R. A. Field and M. I. Gibson, End-Functionalized Poly(vinylpyrrolidone) for Ligand Display in Lateral Flow Device Test Lines, *ACS Polym. Au*, 2022, **2**, 69–79.

24 A. N. Baker, A. R. Muguruza, S. J. Richards, P. G. Georgiou, S. Goetz, M. Walker, S. Dedola, R. A. Field and M. I. Gibson, Lateral Flow Glyco-Assays for the Rapid and Low-Cost Detection of Lectins–Polymeric Linkers and Particle Engineering Are Essential for Selectivity and Performance, *Adv. Healthcare Mater.*, 2022, **11**, 2101784.

25 L. M. Liz-Marzán, Tailoring surface plasmons through the morphology and assembly of metal nanoparticles, *Langmuir*, 2006, **22**, 32–41.

26 Y. Sun and Y. Xia, Gold and silver nanoparticles: A class of chromophores with colors tunable in the range from 400 to 750 nm, *Analyst*, 2003, **128**, 686–691.

27 E. Hao, R. C. Bailey, G. C. Schatz, J. T. Hupp and S. Li, Synthesis and Optical Properties of 'Branched' Gold Nanocrystals, *Nano Lett.*, 2004, **4**, 327–330.

28 P. J. Hernando, S. Dedola, M. J. Marín and R. A. Field, Recent Developments in the Use of Glyconanoparticles and Related Quantum Dots for the Detection of Lectins, Viruses, Bacteria and Cancer Cells, *Front. Chem.*, 2021, **9**, 668509.

29 L. Zhan, S. Z. Guo, F. Song, Y. Gong, F. Xu, D. R. Boulware, M. C. McAlpine, W. C. W. Chan and J. C. Bischof, The Role of Nanoparticle Design in Determining Analytical Performance of Lateral Flow Immunoassays, *Nano Lett.*, 2017, **17**, 7207–7212.

30 B. N. Khlebtsov, R. S. Tumskiy, A. M. Burov, T. E. Pylaev and N. G. Khlebtsov, Quantifying the Numbers of Gold Nanoparticles in the Test Zone of Lateral Flow Immunoassay Strips, *ACS Appl. Nano Mater.*, 2019, **2**, 5020–5028.

31 M. J. Gonzalez-Moa, B. van Dorst, O. Lagatie, A. Verheyen, L. Stuyver and M. A. Biamonte, Proof-of-Concept Rapid Diagnostic Test for Onchocerciasis: Exploring Peptide Biomarkers and the Use of Gold Nanoshells as Reporter Nanoparticles, *ACS Infect. Dis.*, 2018, **4**, 912–917.

32 B. Khlebtsov and N. Khlebtsov, Enhanced solid-phase immunoassay using gold nanoshells: Effect of nanoparticle optical properties, *Nanotechnology*, 2008, **19**, 435703.

33 M. Toyoshima, T. Oura, T. Fukuda, E. Matsumoto and Y. Miura, Biological specific recognition of glycopolymer-modified interfaces by RAFT living radical polymerization, *Polym. J.*, 2010, **42**, 172–178.

34 J. Ishii, M. Toyoshima, M. Chikae, Y. Takamura and Y. Miura, Preparation of glycopolymer-modified gold nano-

35 S. H. Kim, F. L. Kearns, M. A. Rosenfeld, L. Casalino, M. J. Papanikolas, C. Simmerling, R. E. Amaro and R. Freeman, GlycoGrip: Cell Surface-Inspired Universal Sensor for Betacoronaviruses, *ACS Cent. Sci.*, 2022, **8**, 22–42.

36 F. Ahmad, M. M. Salem-Bekhit, F. Khan, S. Alshehri, A. Khan, M. M. Ghoneim, H. F. Wu, E. I. Taha and I. Elbagory, Unique Properties of Surface-Functionalized Nanoparticles for Bio-Application: Functionalization Mechanisms and Importance in Application, *Nanomaterials*, 2022, **12**, 1333.

37 C. L. Schofield, A. H. Haines, R. A. Field and D. A. Russell, Silver and gold glyconanoparticles for colorimetric bio-assays, *Langmuir*, 2006, **22**, 6707–6711.

38 C. L. Schofield, M. J. Marín, M. Rejzek, P. R. Crocker, R. A. Field and D. A. Russell, Detection of mSiglec-E, in solution and expressed on the surface of Chinese hamster ovary cells, using sialic acid functionalised gold nano-particles, *Analyst*, 2016, **141**, 5799–5809.

39 H. Uzawa, K. Ohga, Y. Shinozaki, I. Ohsawa, T. Nagatsuka, Y. Seto and Y. Nishida, A novel sugar-probe biosensor for the deadly plant proteinous toxin, ricin, *Biosens. Bioelectron.*, 2008, **24**, 923–927.

40 R. Karamanska, B. Mukhopadhyay, D. A. Russell and R. A. Field, Thioctic acid amides: Convenient tethers for achieving low nonspecific protein binding to carbohydrates presented on gold surfaces, *Chem. Commun.*, 2005, 3334–3336.

41 S. Watanabe, K. Yoshida, K. Shinkawa, D. Kumagawa and H. Seguchi, Thioglucose-stabilized gold nanoparticles as a novel platform for colorimetric bioassay based on nano-particle aggregation, *Colloids Surf., B*, 2010, **81**, 570–577.

42 H. Otsuka, Y. Akiyama, Y. Nagasaki and K. Kataoka, Quantitative and reversible lectin-induced association of gold nanoparticles modified with α-lactosyl-ω-mercapto-poly(ethylene glycol), *J. Am. Chem. Soc.*, 2001, **123**, 8226–8230.

43 H. Tsutsumi, H. Ohkusa, H. Park, T. Takahashi, H. Yuasa and H. Mihara, Gold nanoparticles conjugated with mono-saccharide-modified peptide for lectin detection, *Bioorg. Med. Chem. Lett.*, 2012, **22**, 6825–6827.

44 L. Ding, R. Qian, Y. Xue, W. Cheng and H. Ju, In situ scano-metric assay of cell surface carbohydrate by glyconanoparti-cle-aggregation-regulated silver enhancement, *Anal. Chem.*, 2010, **82**, 5804–5809.

45 J. X. Xu, M. S. Alom, R. Yadav and N. C. Fitzkee, Predicting protein function and orientation on a gold nanoparticle surface using a residue-based affinity scale, *Nat. Commun.*, 2022, **13**, 7313.

46 C. W. Tornøe, C. Christensen and M. Meldal, Peptidotriazoles on solid phase: [1,2,3]-Triazoles by regios-pecific copper(ɪ)-catalyzed 1,3-dipolar cycloadditions of terminal alkynes to azides, *J. Org. Chem.*, 2002, **67**, 3057–3064.

This journal is © the Partner Organisations 2023

Org. Chem. Front., 2023, **10**, 3819–3829 | **3827**

47 V. v Rostovtsev, L. G. Green, V. v Fokin and K. Barry Sharpless, A stepwise Huisgen Cycloaddition Process: Copper(ɪ)-Catalyzed Regioselective 'Ligation' of Azides and Terminal Alkynes, *Angew. Chem., Int. Ed.*, 2002, **41**, 2596–2599.

48 A. Wang, Y. R. Perera, M. B. Davidson and N. C. Fitzkee, Electrostatic Interactions and Protein Competition Reveal a Dynamic Surface in Gold Nanoparticle-Protein Adsorption, *J. Phys. Chem. C*, 2016, **120**, 24231–24239.

49 X. P. He, Y. L. Zeng, Y. Zang, J. Li, R. A. Field and G. R. Chen, Carbohydrate CuAAC click chemistry for therapy and diagnosis, *Carbohydr. Res.*, 2016, **429**, 1–22.

50 S. Dedola, S. A. Nepogodiev and R. A. Field, Recent applications of the CuI-catalysed Huisgen azide-alkyne 1,3-dipolar cycloaddition reaction in carbohydrate chemistry, *Org. Biomol. Chem.*, 2007, **5**, 1006–1017.

51 R. J. Taylor, M. B. Geeson, T. Journeaux and G. J. L. Bernardes, Chemical and Enzymatic Methods for Post-Translational Protein–Protein Conjugation, *J. Am. Chem. Soc.*, 2022, **144**, 14404–14419.

52 M. Haque, N. Forte and J. R. Baker, Site-selective lysine conjugation methods and applications towards antibody-drug conjugates, *Chem. Commun.*, 2021, **57**, 10689–10702.

53 J. Herzberger, D. Leibig, J. Langhanki, C. Moers, T. Opatz and H. Frey, 'Clickable PEG' via anionic copolymerization of ethylene oxide and glycidyl propargyl ether, *Polym. Chem.*, 2017, **8**, 1882–1887.

54 W. Jian, J. He, Y. Sun and J. Pang, Comparative studies on physicochemical properties of bovine serum albumin-glucose and bovine serum albumin-mannose conjugates formed via Maillard reaction, *LWT–Food Sci. Technol.*, 2016, **69**, 358–364.

55 A. I. Ledesma-Osuna, G. Ramos-Clamont and L. Vázquez-Moreno, Characterization of bovine serum albumin glycated with glucose, galactose and lactose, *Bioconjugate Chem.*, 2008, **29**, 1266–1275.

56 F.-Q. Li, H. Su, X. Chen, X.-J. Qin, J.-Y. Liu, Q.-G. Zhu and J.-H. Hu, Mannose 6-phosphate-modified bovine serum albumin nanoparticles for controlled and targeted delivery of sodium ferulate for treatment of hepatic fibrosis, *J. Pharm. Pharmacol.*, 2009, **61**, 1155–1161.

57 Y. Yang, T. W. Jia, F. Xu, W. Li, S. Tao, L. Q. Chu, Y. He, Y. Li, S. S. Iyer and P. Yu, Fluorescent Neomannosyl Bovine Serum Albumin as Efficient Probe for Mannose Receptor Imaging and MCF-7 Cancer Cell Targeting, *ACS Appl. Nano Mater.*, 2018, **1**, 1058–1065.

58 H. Zhang, D. Laaf, L. Elling and R. J. Pieters, Thiodigalactoside-Bovine Serum Albumin Conjugates as High-Potency Inhibitors of Galectin-3: An Outstanding Example of Multivalent Presentation of Small Molecule Inhibitors, *Bioconjugate Chem.*, 2018, **29**, 1266–1275.

59 C. C. Lee, G. Grandinetti, P. M. McLendon and T. M. Reineke, A polycation scaffold presenting tunable 'click' sites: Conjugation to carbohydrate ligands and examination of hepatocyte-targeted pDNA delivery, *Macromol. Biosci.*, 2010, **10**, 585–598.

60 H. Yu, H. Chokhawala, R. Karpel, H. Yu, B. Wu, J. Zhang, Y. Zhang, Q. Jia and X. Chen, A multifunctional Pasteurella multocida sialyltransferase: A powerful tool for the synthesis of sialoside libraries, *J. Am. Chem. Soc.*, 2005, **127**, 17618–17619.

61 S. Oscarson and A. K. Tidén, Syntheses of the octyl and tetradecyl glycosides of 3,6-di-O-α-D-mannopyranosyl-α-D-mannopyranose and of 3,4-di-O-α-D-mannopyranosyl-α-D-mannopyranose. A new way for 2,4-di-O-protection of mannopyranosides, *Carbohydr. Res.*, 1993, **247**, 323–328.

62 J. A. Harrison, K. P. R. Kartha, E. J. L. Fournier, T. L. Lowary, C. Malet, U. J. Nilsson, O. Hindsgaul, S. Schenkman, J. H. Naismith and R. A. Field, Probing the acceptor substrate binding site of Trypanosoma Cruzi trans-sialidase with systematically modified substrates and glycoside libraries, *Org. Biomol. Chem.*, 2011, **9**, 1653–1660.

63 C. M. Keyari and R. Polt, Serine and threonine Schiff base esters react with β-anomeric peracetates in the presence of BF₃·Et₂O to produce β-glycosides, *J. Carbohydr. Chem.*, 2010, **29**, 181–206.

64 C. Bensoussan, N. Rival, G. Hanquet, F. Colobert, S. Reymond and J. Cossy, Iron-catalyzed cross-coupling between C-bromo mannopyranoside derivatives and a vinyl Grignard reagent: Toward the synthesis of the C31–C52 fragment of amphidinol 3, *Tetrahedron*, 2013, **69**, 7759–7770.

65 V. L. Campo, I. Carvalho, S. Allman, B. G. Davis and R. A. Field, Chemical and chemoenzymatic synthesis of glycosyl-amino acids and glycopeptides related to Trypanosoma cruzi mucins, *Org. Biomol. Chem.*, 2007, **5**, 2645–2657.

66 K. Hirayama, S. Akashi, M. Furuya and K.-I. Fukuhara, Rapid Confirmation and revision of the primary structure of bovine serum albumin by ESI-MS and FRIT-FAB LC/MS, *Biochem. Biophys. Res. Commun.*, 1990, **173**, 639–646.

67 X. Cui, M. Liu and B. Li, Homogeneous fluorescence-based immunoassay via inner filter effect of gold nanoparticles on fluorescence of CdTe quantum dots, *Analyst*, 2012, **137**, 3293–3299.

68 P. T. Nyffeler, C. H. Liang, K. M. Koeller and C. H. Wong, The chemistry of amine-azide interconversion: Catalytic diazotransfer and regioselective azide reduction, *J. Am. Chem. Soc.*, 2002, **124**, 10773–10778.

69 S. I. Presolski, V. P. Hong and M. G. Finn, Copper–Catalyzed Azide–Alkyne Click Chemistry for Bioconjugation, *Curr. Protoc. Chem. Biol.*, 2011, **3**, 153–162.

70 H. P. Erickson, Size and shape of protein molecules at the nanometer level determined by sedimentation, gel filtration, and electron microscopy, *Biol. Proced. Online*, 2009, **11**, 32–51.

71 Y. Wang, G. Yu, Z. Han, B. Yang, Y. Hu, X. Zhao, J. Wu, Y. Lv and W. Chai, Specificities of Ricinus communis agglutinin 120 interaction with sulfated galactose, *FEBS Lett.*, 2011, **585**, 3927–3934.

72 B. P. Peters, S. Ebisu, I. J. Goldstein and M. Flashner, Interaction of Wheat Germ Agglutinin with Sialic Acid, *Biochemistry*, 1979, **18**, 5505–5511.

3828 | *Org. Chem. Front.*, 2023, **10**, 3819–3829

This journal is © the Partner Organisations 2023

73 J. H. Naismith and R. A. Field, Structural basis of trimannoside recognition by concanavalin A, *J. Biol. Chem.*, 1996, **271**, 972–976.

74 S. K. Bikkarolla, S. E. McNamee, P. Vance and J. McLaughlin, High-Sensitive Detection and Quantitative Analysis of Thyroid-Stimulating Hormone Using Gold-Nanoshell-Based Lateral Flow Immunoassay Device, *Biosensors*, 2022, **12**, 182.

75 B. Srinivasan, D. M. Nanus, D. Erickson and S. Mehta, Highly portable quantitative screening test for prostate-specific antigen at point of care, *Curr. Res. Biotechnol.*, 2021, **3**, 288–299.

76 H. Shinchi, N. Yuki, H. Ishida, K. Hirata, M. Wakao and Y. Suda, Visual detection of human antibodies using sugar chain-immobilized fluorescent nanoparticles: Application as a point of care diagnostic tool for Guillain-Barré syndrome, *PLoS One*, 2015, **10**, e0137966.

This journal is © the Partner Organisations 2023

Org. Chem. Front., 2023, **10**, 3819–3829 | **3829**